J Infrared Milli Terahz Waves (2011) 32:513–527
DOI 10.1007/s10762-011-9769-6

Non-Destructive Measurement of Water Diffusion in Natural Cork Enclosures Using Terahertz Spectroscopy and Imaging

Anthony J. Teti · David E. Rodriguez · John F. Federici · Caroline Brisson

Received: 3 January 2011 / Accepted: 10 February 2011 /
Published online: 19 February 2011

Abstract Terahertz (THz) imaging enables non-destructive evaluation of many materials' internal structures which could not be probed by visual analysis alone. In this paper, we apply THz imaging to non-destructively probe and image the diffusion of water through natural cork samples. The temporal and spatial distribution of water is analyzed as it diffuses throughout the cork structure. An average diffusion coefficient comparable to previous work in the field is extracted from this analysis. Data is also presented to show that the diffusion coefficient is not uniform throughout the cork but changes dramatically due to the local structure and composition of the cork.

Keywords Terahertz · Non-destructive evaluation · Wood · Cork · Diffusion

1 Introduction

Terahertz (THz) spectroscopy and imaging [1] has received considerable attention for non-destructive evaluation of various materials including polymers, pharmaceuticals [2], detection of concealed weapons, and explosives [3, 4]. The technique has also been applied to non-destructive evaluation of moisture content in grain [5, 6], leaves [7–9], wood [10], as well as polymers [11, 12]. In a previous paper, we introduced Terahertz (THz) spectroscopy and imaging as a non-destructive evaluation tool of natural cork enclosures [13]. Natural cork is acquired from the Cork Oak (Quercus suber) which grows predominately in Portugal and other countries surrounding the Mediterranean Sea. It is utilized in a variety of products including cork stoppers for wine and other beverages. As an enclosure for liquids, it has the desirable properties of being largely impermeable to liquids and gases, as well as compressible [14].

A. J. Teti · D. E. Rodriguez · J. F. Federici (✉)
Department of Physics, New Jersey Institute of Technology, Newark, NJ 07102, USA
e-mail: federici@adm.njit.edu

C. Brisson
Department of Engineering Physics, Ramapo College of New Jersey, Mahwah, NJ 07430, USA

With natural cork as well as polymers and pharmaceuticals, the permeability or diffusion of liquids and gases is an important issue. As examples, the performance of controlled delivery pharmaceutical products is partially determined by the diffusion of solvents into their polymeric coatings. Likewise, the characterization of water diffusion in wood plastic composites, due to their use in construction applications, is essential. In the case of natural cork, the large volume of the cork cell lumen and relatively low humidity enables the material to be compressible, yet exhibit fairly high THz transmission. However, as the cork absorbs liquids such as water, the intrinsically high THz absorbance of liquids enables THz imaging to follow the progression of the liquid as it permeates and diffuses through the cork structure.

The diffusion of water in natural corks is anisotropic [14] in the radial, axial and tangential directions. The radial direction corresponds to the direction of the radial growth of the Cork Oak tree. The axial direction is parallel to the tree's axis. The transverse direction corresponds to the direction along the circumference of the tree's diameter. The anisotropy in diffusion can be attributed to several effects. For example, it is well-known [14, 15] that the diffusion coefficient in the radial growth direction is larger than that of the other two directions due to the presence of lenticular channels (pores) that run parallel to the radial growth direction. The lenticular channels enable water and gases to diffuse through the cork. In addition, one would expect the presence of cracks, voids, and defects to increase the diffusion. The presence of these potentially highly anisotropic features in the cork implies a highly variable *local* diffusion rate. The extraction and migration of volatile chemicals from the cork [16] will depend on the local diffusion rates and the presence of volatiles in the area of contact between the wine and the cork.

THz time-domain spectroscopy has been used to measure the diffusion of solvents in polymeric materials. Reference [12] describes measurements of water absorption and diffusion in polyamide and wood plastic composite using THz time-domain spectroscopy. With polymers as well as natural cork, one can use THz spectroscopy to differentiate between bound water (water molecules bound to the sample material) or free liquid water. The dielectric properties of bound and free water differ due to the fact that the molecules' vibrations are slightly altered by their local environment. In particular, bound water has a lower refractive index and absorption coefficient compared to free water. As described in Ref. [12], the diffusion is modeled using the weight percent increase in the sample

$$Wt\%(t) = K\, t^m \tag{1}$$

where K and m are constants and t is time. When $m = 1/2$, the diffusion follows Fick's diffusion equations. A fit of the measured total water absorption versus time in polyamide follows the Fick diffusion model with a diffusion coefficient of 3.4×10^{-13} m^2/s.

THz spectroscopy has also been used to measure the diffusion of acetone in polycarbonate and polyvinylchloride polymers [17]. In these measurements, a THz reflection geometry is used to track the progression of the dry polymer/liquid interface over time. Pulses of THz radiation reflect from dry polymer/liquid interface. As the boundary of the diffusing liquid moves through the material, the reflecting pulses are detected earlier in time indicating motion of the liquid. In analyzing the kinetics of the wavefront, Ref. [17] uses a similar equation to Eq. 1: Since the liquid absorption is typically correlated with the front position of the penetrating liquid, one may replace the left hand side of Eq. 1 with the time dependant depth of penetration of the liquid to analyze the diffusion.

There are several methods for determining the diffusion coefficient of water in natural corks [14]. In the first method, small cork samples are submerged in water. As a function of

time, the samples' dimensions and mass are measured to determine the samples' change in volume and mass due to the diffusion of water into the cork. From these measurements, Rosa and Fortes [15] conclude that the water predominately diffuses along the walls of the cork cell until the change in weight relative to the dry cork weight is approximately 60%. While water can accumulate into the interior of the cork cell via evaporation/condensation, this process only dominates after the cell walls are saturated.

A second method of determining the diffusion of water in cork involves inserting two metallic electrodes into the cork and measuring the electrical resistance between them [15, 18]. One side of the sample is placed in contact with a water reservoir. As time evolves, water diffuses from the reservoir into the cork's structure. If water were absent from the proximity of the electrodes, the resistance would be very high. As the concentration of water increases between the two electrodes, the resistance dramatically decreases.

In a third method, nuclear magnetic resonance (NMR) microscopy is used to image the diffusion of water into natural cork [19]. The results of Ref. [19] suggest that after three days, the absorption of water is limited to the lenticels of the cork. In those samples, the lenticular channels have diameters between 1.0–1.5 mm.

There are two inherent limitations with the first two established techniques: (a) they are inherently invasive detection methods and (b) they measure essentially average diffusion properties. In the cork submersion method, samples must be continually removed from the soak in order to record data. Using the electrical method, the cork structure must be punctured. Both methods measure average sample properties: The cork submersion method measures the total volume and weight change of the sample. Some degree of localized measurement is possible with the electrical method by using multiple sets of electrodes. However, a spatially continuous measurement is not possible. The electrode method is particularly troublesome since the shape of the resistance versus time curves depends upon the depth of the electrode placement in the cork [15]—an artifact of the inhomogeneity of the cork. Consequently, the electrode technique does not show an appreciable anisotropy in the radial and non-radial diffusion coefficient whereas the submersion measurement does show roughly a factor of 4.3 difference.

In this paper, we apply THz spectroscopy and imaging to measure not only the average diffusion coefficients for a cork sample, but also image the localized presence of water in the cork structure to produce time-dependant images of water propagation in the cork structure. Unlike the methods described above in which cork samples are carefully selected to eliminate obvious cracks, defects, or voids in the sample, the THz method does not require an a-priori selection of cork sample in order to measure the average diffusion coefficients. Moreover, the THz imaging enables one to visualize and characterize the effect of lenticels, cracks, voids, and defects on the local diffusion of water.

The paper is organized as follows: Section 2 describes experimental setup. Section 3 describes the analytical manipulation of the data and presents time-dependant images of the water diffusion through the cork structure. The imaging results are discussed in Section 4 as well as the localized and averaged diffusion coefficients. The important results of this study are summarized in Section 5.

2 Experimental setup

Natural cork samples were obtained from wine stoppers that had been dried in ambient air for several days. The samples were cut from the side that had not been in contact with the wine. Two types of samples were studied: Circularly shaped samples cut

parallel to the circular cross-section of the cork stopper and rectangular shaped samples cut parallel to the long axis of the cork stopper. Natural cork stoppers are manufactured such that the long axis of the cork corresponds to the axial direction of cork tree growth whereas the circular cross-section includes both the radial grown direction and the tangential growth direction which is parallel to the grain in the cork [14]. Typical circular samples have a radius and thickness of 10.5 mm and 4 mm, respectively. The axial samples have dimensions of 16 mm parallel to the axial direction, 14 mm width and a thickness of 5 mm. For measurements of diffusion in the circular cross-section, the cork sample was enclosed between two sapphire windows using parafilm to only allow water absorption along the circumference of the sample. The sapphire windows/cork sample is encased in heat-shrink tubing to make a waterproof enclosure. Distilled water was injected into the enclosure to keep the cork submerged. For diffusion measurements along the long axis of the cork, a similar approach was taken to prepare the sample. In addition to the parafilm to prevent water penetration into the cork along the sapphire window surface, the surface of the cork was sealed using a water proof glue to prevent any water entry through the cork surface perpendicular to the axial direction. A circular cork sample and enclosure are shown in Fig. 1.

Terahertz spectral images were acquired using the Picometrix T-Ray 2000 system as described in our previous work [13]. Acquisition of a THz image of the sample required approximately 1 hour. An image of the dry cork sample is first recorded. Subsequent to the injection of water into the sample holder, THz images are recorded continuously every hour. Prior to the acquisition of each THz image, the cork sample is translated out of the THz beam path and a background time-domain scan is recorded. The pixel size of the images is typically 0.3 mm.

3 Data analysis

For each pixel in the image, the THz frequency dependant absorbance is calculated:

$$A(\nu) = -\ln(T(\nu)) = -\ln\left(\frac{|E_s(\nu)|}{|E_r(\nu)|}\right) \tag{2}$$

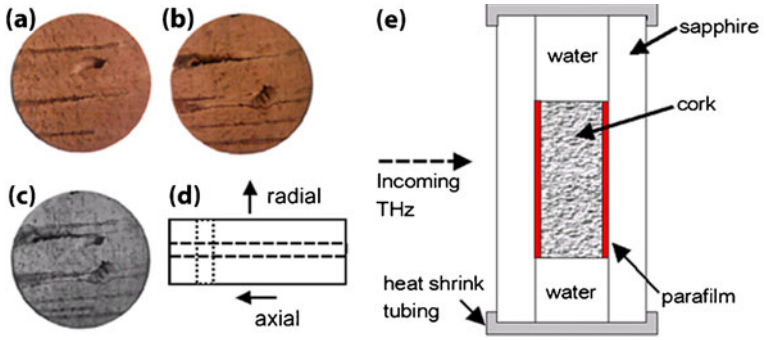

Fig. 1 Visible images of cork cross sections for **a** front and **b** back surfaces. The back surface image is flipped horizontally so that the composite image **c** can be used to visualize the composite structure of the two surfaces in transmission. **d** illustration of the cuts for the circular (*dotted lines*) and rectangular (*dashed lines*) cork samples relative to the growth directions of the cork oak. **e** A schematic of the sample enclosure.

where $|E_r(\nu)|$ and $|E_s(\nu)|$ are the magnitudes of the reference and sample THz electric fields as calculated by the Fourier transform of the time-domain data, and $T(\nu)$ is the transmission through the sample as a function of the THz frequency ν. To obtain a single value at each pixel position and construct an image, the absorbance is averaged over a narrow bandwidth.

The optimal bandwidth for image processing is determined by two factors: spatial resolution and signal-to-noise. Since the higher frequencies of THz radiation can be focused to smaller spot sizes due to diffractive effects, one generally realizes better spatial resolution in the THz images as the THz frequency increases. However, the signal-to-noise ratio drops dramatically as the THz frequency increases. Consequently, there is a trade-off between spatial resolution and signal-to-noise. To determine an effective compromise, we examine the THz spectra in a region of cork after ~95 hours of soaking. The noise limit of our system is determined by placing a metal plate in front of the THz detector during a time-domain scan. This scan represents the noise limit of our system when no THz radiation reaches the detector. The range from 0.65–0.70 THz is chosen as the spectral bandwidth for data processing: the THz frequency is high enough to provide good spatial resolution (~0.3 mm) with adequate signal-to-noise.

Once the cork absorbance images are created for each time interval, the images are combined to create a time-lapsed movie that shows the diffusion of water through the corks. Montages of the resulting movies for both the circular cross-section and axial cork samples are shown in Figs. 2 and 3, respectively. Note that the area surrounding the cork initially has low absorbance. After the introduction of water, this area becomes highly absorbing. The cork sample in Fig. 2 is oriented so that the radial direction of cork growth is parallel to the bottom of the page. The tangential growth direction is perpendicular to the bottom of the page. Note that while the cork sample is circularly shaped, the diffusion of water does not exhibit radial symmetry due to the varying diffusion rates in the different growth directions. Clearly, the diffusion of water is more rapid in the radial direction of tree growth compared to the tangential direction. It is also clear in comparing Figs. 1 and 2 that the lenticels and cracks/voids quickly fill with water therefore dominating the diffusion of water. This behavior is consistent with previous water diffusion measurements using NMR

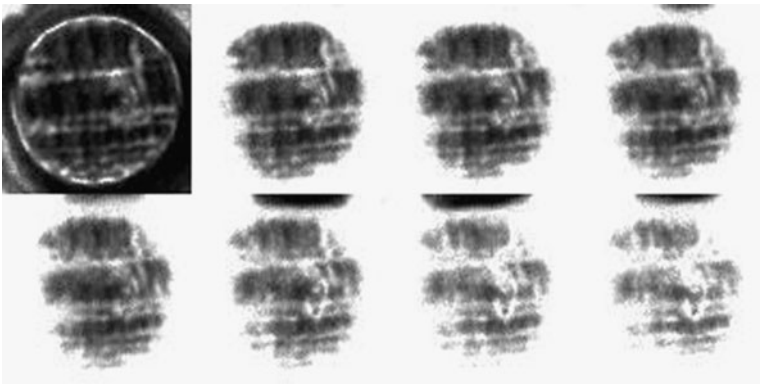

Fig. 2 THz absorbance (0.65–0.7 THz) through cork cross-section at 0 hr (dry cork), 10.9 hr, 21.9 hr, 33 hr, 44 hr, 55.6 hr, 78.2 hr, and 93.6 hr, respectively. Dark regions correspond to low absorbance while light blue regions correspond to high absorbance. Regions outside of the cork are highly transparent in the dry image since the water had not been added to the sample chamber. Dark regions near the top of the sample chamber result from the level of water dropping in the chamber due to evaporation.

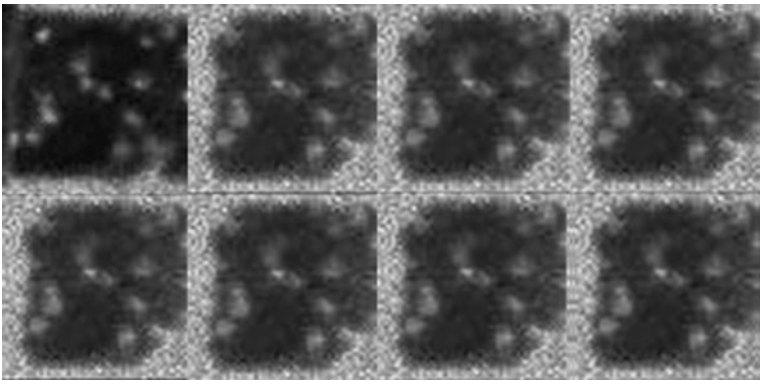

Fig. 3 THz absorbance (0.65–0.7 THz) through cork cross-section at 0 hr (dry cork), 1.75 hr, 5.25 hr, 25.25 hr, 51.25 hr, 56.75 hr, 144 hr, 316.5 hr, respectively. Dark regions correspond to low absorbance while bright regions correspond to high absorbance. The lenticels are bright (corresponding to high attenuation) in the dry image due to efficient scattering of the THz radiation by the boundaries of the channel.

[19]. In contrast, the cork sample of Fig. 3 is oriented so that the axial growth direction is parallel to the bottom of the page while the radial growth direction is perpendicular to the plane of the page. In the dry cork image, the lenticels appear as bright spots in the interior of the cork due to significant scattering of THz radiation by the edges of the lenticular channels. Once water is added to the sample chamber, the diffusion in the axial growth direction is comparatively much slower than the diffusion shown in Fig. 2.

In order to create images which only show the flow of water through the cork, the dry cork images are subtracted from the data of Figs. 2 and 3 thereby removing the absorbance due to the dry cork features and only leaving the absorbance of the water inside the cork. The movie montages for the radial and axial water only diffusion are shown in Figs. 4 and 5, respectively. Clearly the water diffuses much more rapidly in the radial growth direction compared to the axial growth direction of the cork.

Previous THz measurements of solvent diffusion in polymers used a reflection geometry to track the diffusion wave-front [17]. In our transmission configuration, we can also extract the location of the wavefront by processing the images of Figs. 4 and 5 to monitor which

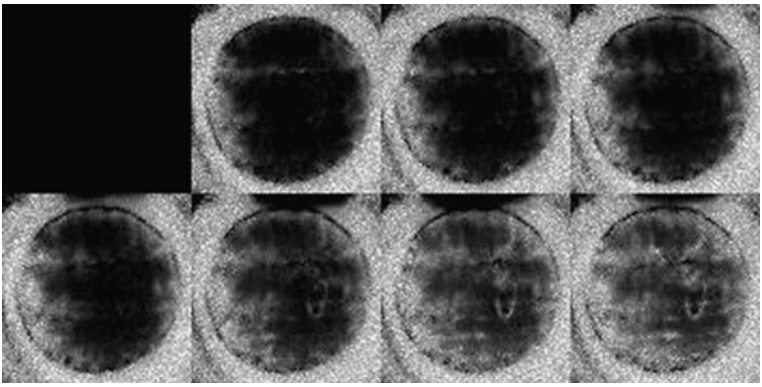

Fig. 4 Water-only diffusion (dry cork image subtracted) through the cork of Fig. 2.

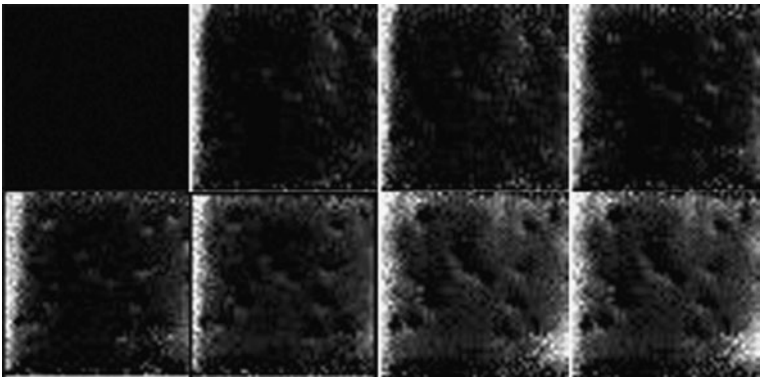

Fig. 5 Water-only diffusion (dry cork image subtracted) through the cork of Fig. 3.

pixels exhibit an absorbance value above a fixed threshold. As will be shown below, one can relate the THz absorbance value to the concentration of water in the cork. The images are segmented into binary images with an absorbance threshold of 0.5 (corresponding to 12% by weight water for a 4 mm thick sample) for Fig. 4 and an absorbance threshold of 0.3 (5.7% by weight water for a 5 mm thick sample) for Fig. 5 as shown in Figs. 6 and 7, respectively. The correspondence between absorbance threshold and water weight will be discussed in the next section and Fig. 9.

4 Discussion

As can be seen from Fig. 6, water diffusion in the radial growth direction is much faster than along the tangential direction. This is consistent with the cork submersion study by Rosa and Fortes [15]. Rosa and Fortes attribute this effect to the alignment of the cell wall which allows more flow in the radial direction as well as the presence of lenticular channels aligned in the radial direction, which will contribute to faster diffusion [15]. As can be seen in Fig. 7, the rapid diffusion of water in the lenticular channels is mitigated since the

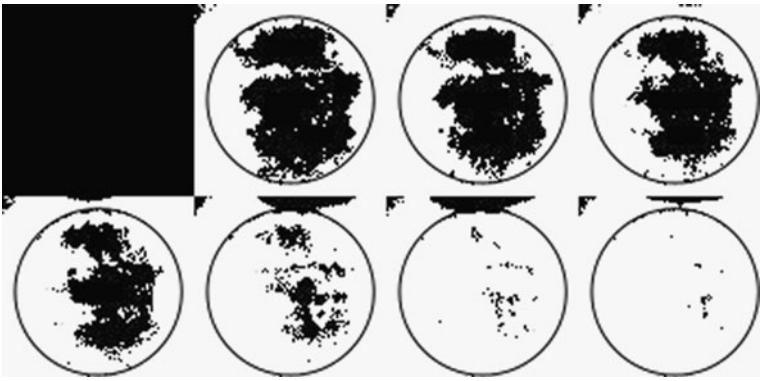

Fig. 6 Tracking of the diffusion front using a 0.5 absorbance threshold. An absorbance of 0.5 through the 4 mm sample corresponds to 12% weight increase of water. The dark circle indicates the location of the sample.

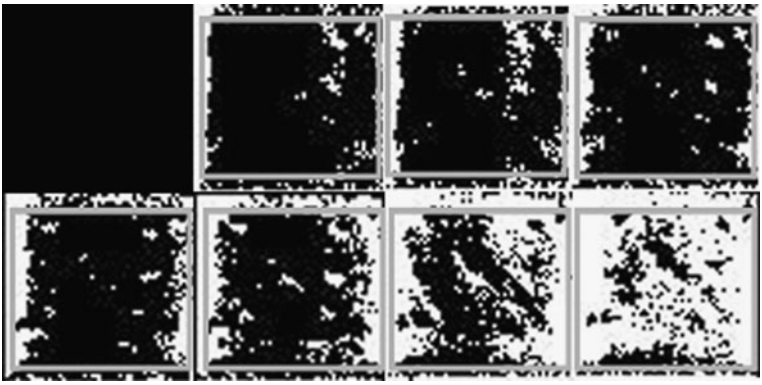

Fig. 7 Tracking of the diffusion front in the axial growth direction using a 0.3 absorbance threshold. An absorbance of 0.3 through a 5 mm sample corresponds to 5.7% weight increase in water. The gray rectangle indicates the location of the sample.

predominate flow of water is in the axial direction: Even though the channels can quickly fill with water, they are spatially isolated from each other in the axial direction resulting in a lower average diffusion coefficient compared to Fig. 6.

In order to extract a diffusion coefficient for the cork, one needs to establish a relationship between the measured THz absorbance and the concentration of water in the cork. To extract this relationship, one needs to know the frequency dependant dielectric permittivity of the cork, as well as water, and use a model to predict the effective dielectric properties of wet cork in the THz range as a function of water content. It is known that the cell walls of cork reach saturation when the weight of the initially dry cork increases by 60% relative to the dry cork weight [15]. Based on their data, Rosa and Fortes conclude that water predominately diffuses through the cork via the cork cell walls before it fills the internal volume of the cork cell. In this paper, we will use the 60% weight increase as the threshold for determining the diffusion coefficient of the cork. As will be shown below, the THz absorbance values suggest that we are below the saturation point on average throughout the cork.

In order to model the effective dielectric properties of mixtures in the Terahertz range, several methods have been proposed [20]. As an example, Ref. [11] modeled the presence of water in polymer via a linear model for the effective absorption coefficient α and the volume fraction of water X :

$$\alpha_{eff}(\nu) = (1 - X)\alpha_h(\nu) + X\alpha_w(\nu) \tag{3}$$

where *eff* stands for the effective medium, *h* stands for the host medium and *w* stands for the water. Other effective medium models include the Landau, Lifshitz, and Looyenga (LLL) model—derived in the limit of low dielectric contrast mixtures—in which the dielectric permittivity ε is modeled as

$$\sqrt[3]{\varepsilon_{eff}} = (1 - X)\sqrt[3]{\varepsilon_h} + X\sqrt[3]{\varepsilon_w}. \tag{4}$$

The complex dielectric permittivity is related to the real refractive index n and absorption coefficient α through

$$\varepsilon = \varepsilon_r - i\varepsilon_i = \left[n^2 - \left(\frac{\alpha\lambda}{2\pi}\right)^2\right] - i\left[n\frac{\alpha\lambda}{\pi}\right] \tag{5}$$

where n is the real index of refraction, λ is the vacuum wavelength of the radiation, and α is the absorption coefficient of the THz electric field. (The absorption coefficient of power is 2α.)

To determine the weight percentage of water in the cork and corresponding THz absorbance, we model the THz absorbance of the cork using Garnett effective medium theory [21]. Garnett theory calculates the effective dielectric properties of a material formed by the presence of small (spherical) particles embedded in a host material:

$$\frac{\varepsilon_{eff} - \varepsilon_h}{\varepsilon_{eff} + 2\varepsilon_h} = X \frac{\varepsilon_p - \varepsilon_h}{\varepsilon_p + 2\varepsilon_h} \tag{6}$$

In the case of dry natural cork, the host material is that of the cell wall with the embedded particles being the cell lumen (ie. empty space inside of the cell walls). Typically, uncompressed cork cells are 80–95% empty space.

From our previous paper [13], we estimate that the refractive index of cork to be 1.1 while the frequency dependant absorbance can be written as

$$A(\nu) = C\,\nu^m + B. \tag{7}$$

where C=0.792, m=1.13, B=0.09 are typical values for spring growth cork cells which are 4.4 mm thick, and ν is in units of THz. If we treat natural cork as an effective medium comprised of host material of cell walls with air "particles" intermixed in the host material, we can then determine the effective dielectric permittivity of cork (Eq. 6) using n=1.1 and the absorption coefficient of Eq. 7. Using this effective permittivity, the dielectric constant of air (ε_p=1), and the assumption that the air "particles" comprise 65% of the cork cell volume, one can use Eq. 6 to estimate that the dielectric permittivity of the cork cell walls as shown in Fig. 8. A value of 65% air compared to 80–90% for normal cork is used to account for the fact that the samples of Ref. [13] and in the present work were compressed from being used as stoppers.

From the calculated dielectric permittivity of the cork cell walls, we now estimate the effective dielectric permittivity of a water absorption by the cork cell walls by treating the dry cell wall dielectric permittivity (Fig. 8) as the "host" material and water as the "particles". The overall dielectric permittivity of wet natural cork then is calculated using a "host" material of wet cell walls embedded with "particles" of air. Based on these calculations, the net change in the absorbance of a 4 mm thick wet natural cork relative to dry natural cork as a function of water content is shown in Fig. 9. Note that the 60% by weight saturation threshold corresponds to an absorbance level of roughly 2.76. In order to test the correspondence between the absorbance and % water weight, ten samples of cork were soaked in water. Periodically, the average THz absorbance through the samples and percent water weight of the samples are recorded. The values for ten samples are shown as open square symbols in Fig. 9.

Clearly, detailed modeling of the effective dielectric of natural cork is more complicated than presented here. For example, the cork cell is not spherical (as is assumed in the Garnett model) but rather a Kelvin polyhedron [14]. While more complicated models of the effective dielectric properties of materials exist, [20] the Garnett theory is sufficient for our application since the Kelvin polyhedron more closely resembles a sphere than a long tube or flat disk. The LLL model—which is shape independent—only applies if the difference in the dielectric values of the host and particles is small. For wet cork cells, there is a large dielectric mismatch between the air of the cell lumens and the dielectric value of the water or cell wall. In addition, our model does not differentiate between cell structure from spring or autumn growth of the cork oak tree. Nor do we explicitly take into account the presence of lenticels, cracks, or voids in calculating Fig. 9. Lastly, we do not include the small

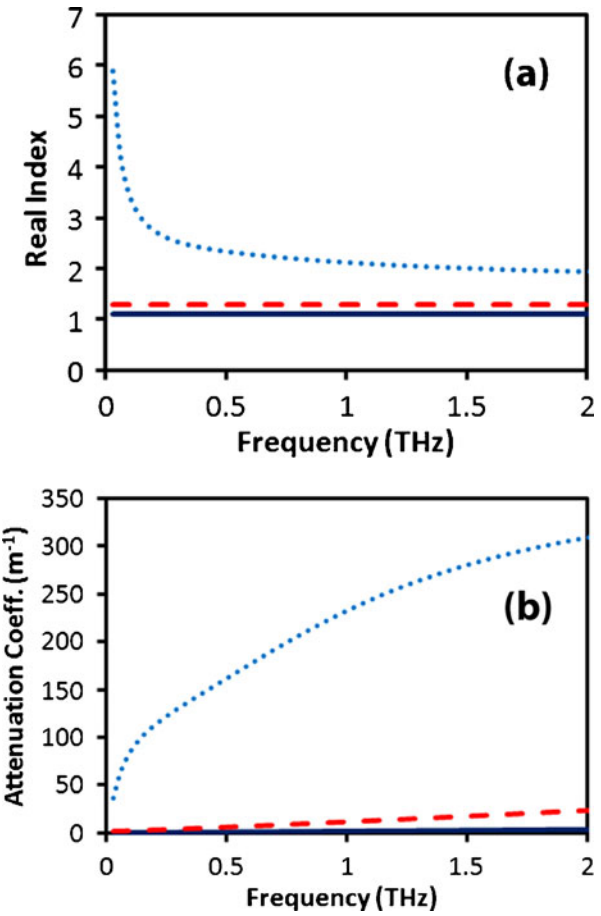

Fig. 8 **a** Frequency dependant real indices of refraction of natural cork (*solid*) from Eq. 7 and the data of Ref. [13], unbounded water (*dots*) from the Debye model [22], and calculated cork cell wall (*dashed*) from Eq. 6. **b** Corresponding power attenuation coefficients.

correction between bound water (water molecules bound to the sample material) and free liquid water. Therefore, the change in absorbance versus percent weight of water in Fig. 9 should be interpreted as an approximation which will be used to predict the effective diffusion coefficient of the natural cork.

As an initial check on our THz imaging analysis, we compare previously published diffusion values for cork to an effective diffusion coefficient which we extract from the THz imaging data for the entire cork disk. For this comparison, we model the diffusion processes using the Fick equation for diffusion through an isotropic disk with a constant fluid concentration at its boundary [23]:

$$\frac{M_t}{M_\infty} = 1 - \sum_{n=1}^{\infty} \frac{4}{a^2 \sigma_n^2} \cdot e^{-D\sigma_n^2 (t - t_0)} \tag{8}$$

$$\{\sigma_n | J_0(a \cdot \sigma_n) = 0\}$$

where M_t and M_∞ are the amount of diffusing water at time t and $t{=}\infty$, respectively. The disk has a radius a and an effective diffusion coefficient D. The variable σ_n is the n-th root of the

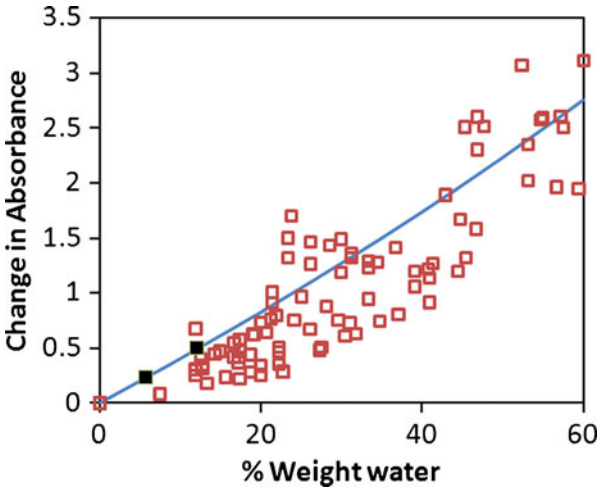

Fig. 9 Calculated change in absorbance at 0.65–0.7 THz of wet cork relative to dry cork as a function of % weight of water relative to the weight of a dry cork (*solid line*). The thickness of the cork is 4 mm. The points corresponding to 0.5 absorbance with a 12% weight increase of water (Fig. 6) in a 4 mm sample and 0.3 absorbance with a 5.7% weight increase in a 5 mm thick sample are indicated by the solid squares. The open squares correspond to measured values of absorbance versus percent water weight for 10 cork samples. While there is significant sample to sample variations, the measured absorbance values are consistence with those predicted by Garnett effective medium theory.

zeroth order Bessel function of the first kind. For the analysis, we assume that the values of M can be represented by the average THz absorbance of the cork sample with M_∞=2.76 corresponding to fully saturated (60%) cork cell walls.

Using the data of Fig. 2, the ratio M/M_∞ averaged over the entire cork versus time is calculated (Fig. 10). The Absorbance fraction is converted to a % weight fraction of water using Fig. 9. A best fit to Fig. 10 using Eq. 8 yields an effective diffusion coefficient of 1.8×10^{-11} m^2/s. This value is comparable to the value determined by Rosa and Fortes using the cork immersion method [15]. A similar analysis of the axial diffusion of Fig. 5 yields an

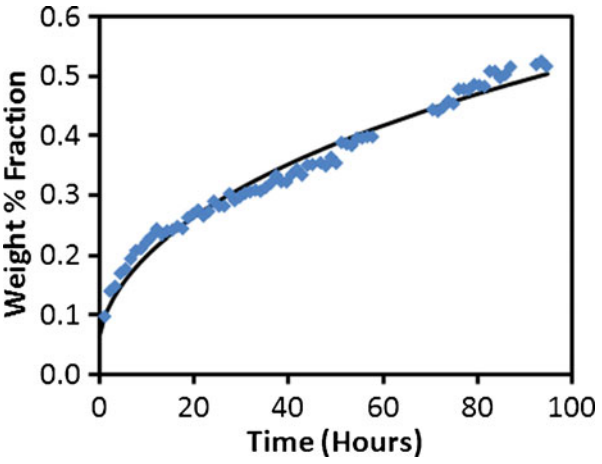

Fig. 10 Measured % weight fraction (relative to 60%) versus time averaged over entire cork. The solid line is a best fit to the experimental data using Eq. 8 *with* a diffusion coefficient of 6.5×10^{-4} cm^2/hr (1.8×10^{-11} m^2/s).

effective axial diffusion coefficient roughly a factor of 7 smaller than that calculated for the circular cross-section of cork. This result is qualitatively consistent with the immersion measurements of Rosa and Fortes who show that non-radial diffusion is roughly a factor of 4 smaller than radial diffusion.

While averaging of the THz absorbance data over the entire cork yields an effective diffusion coefficient which is comparable to values measured by other means, THz imaging offers the advantage compared to these other measurement techniques of producing time dependant images of the diffusion of liquid through the cork structure. Diffusion throughout the cork is not uniform as can be seen in Figs. 6 and 7. The inhomogeneity of the cork (e.g. due to cracks, voids, lenticular channels) implies that there will be local variations in the diffusion coefficient. An analysis on multiple regions of the cork was performed to illustrate this point. Figure 11 (and Fig. 1c) shows a composite visible image of the front and back surfaces of the cork sample as well as the corresponding THz absorbance image of dry cork in the 0.65–0.7 THz range. The regions for localized analysis—labeled 0 to 9—are indicated in the THz image. Region 1 and 2 correspond to large channels in the cork. Region 3 corresponds to a pristine region of cork which only absorbs water after a long time. Region 4 corresponds to a crescent shaped empty cavity in the cork which was intentionally created with a cork screw. Regions 5–8 correspond to grain structure in the cork. Regions 5 and 8 correspond to grains with enhanced THz absorbance compared to Regions 6 and 7. Regions 9 and 0 are adjacent locations near the edge of the cork. Region 0 is in a channel while Region 9 lies just outside of the channel.

At each position in Fig. 11—analogous to the analysis which produced Fig. 10—the average absorbance between 0.65–0.7 THz is calculated as a function of time. In order to smooth the resulting absorbance data, values within one pixel of the center positions are averaged together. The dry cork absorbance value at that location is subtracted from the data. Lastly, the absorbance data is normalized to the 60% saturated water value of 2.78. The corresponding absorbance fraction corresponds to the presence of water in the cork structure.

The resulting curves for Regions 1–4 are plotted in Fig. 12. In comparing Regions 1 and 2 which are located inside of channels, there is an initial rapid rise in the absorbance due to water in the first few hours. This is consistent with NMR observations [19] that water quickly fills the lenticular channels of cork as well as observations by Fortes and Rosa that water quickly is quickly absorbed by the boundaries of the cork [15]. It is also interesting that there appears to be a "time delay" of ~7 hours in the onset of absorbance in Region 1 compared to Region 2. We attribute this delay to the fact that Region 2 is closer to the surface of the cork while Region 1 is further in the interior of the channel and would require the water to travel a longer distance to reach the interior of the channel.

Region 4 which includes a cavity within the cork shows interesting behavior. From 0–40 hours, there is a slow increase in the concentration of water. After ~45 hours, there is

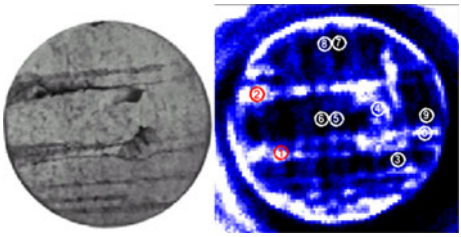

Fig. 11 (*left*) Composite visible image of front and back surfaces of cork sample. (*right*) THz absorbance (0.65–0.70 THz) through dry cork. Regions labeled 0 through 9 are analyzed for the local change in absorbance with time as the water diffuses thorough the cork.

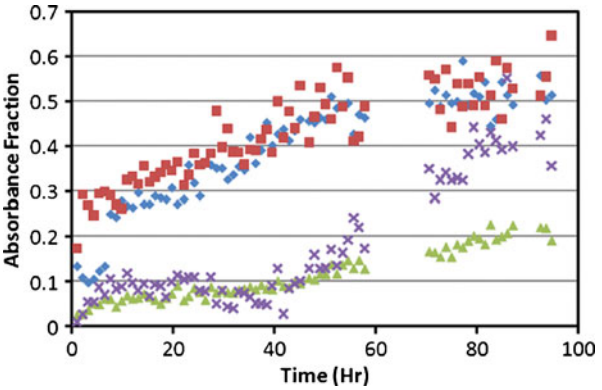

Fig. 12 Absorbance fraction versus time for Regions 1 (*diamond*), 2 (*square*), 3 (*triangle*) and 4 (X).

a rapid increase in the absorbance. As is shown in Fig. 4, at this time, water begins to noticeably fill in the crescent shaped void in the cork. Therefore, it seems reasonable that prior to 40 hours, the water is predominately diffusing via cork cell walls into Region 4. After 40 hours, the crescent shaped void begins to fill with water resulting in a large increase in THz absorbance. Region 3 corresponds to a region of cork which takes a long time to absorb water. Note that in Regions 3 and 4 that the THz absorbance (and concentration of water) very gradually increases with time prior to 40 hours. However, since Region 3 is free of voids in the cork, there is not a dramatic increase in the absorbance after 40 hours as there is in Region 4.

A comparison of the normalized absorbance inside of a lenticular channel (Region 0) to a nearby location outside of the channel (Region 9) is shown in Fig. 13. As with Regions 1 and 2, there is an immediate increase in the absorbance due to the diffusion of water into these regions close to the cork's surface. However, Region 0 in the channel shows a larger absorbance and water concentration for $t<10$ hours. Since Regions 0 and 9 are located near each other, the presence of a large water concentration in Region 0 will induce a large flux of water flowing into Region 9. At $t=20$ hours, there is no longer a large gradient in the water concentration between the two regions resulting in commensurate concentrations of water in the two regions.

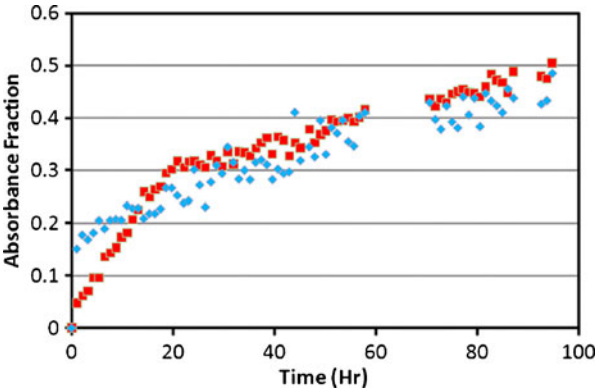

Fig. 13 Absorbance fraction versus time for Region 0 (*diamond*) and 9 (*square*).

In Fig. 14, we compare the time evolution of the absorbance fraction of the grain structure in the cork. Regions 5 and 6 correspond to "light" and "dark" grains near the middle of the cork sample while Regions 8 and 7 correspond to similar grains near the top of the cork structure. Note that all the grain locations behave essentially the same prior to t=40 hours. After 40 hours, there is a dramatic increase in the rate of water diffusion into these regions. As with Fig. 12, we attribute this sudden change to the filling of the crescent void near Region 4. The large concentration of water in the void creates a large gradient in the concentration of water relative to nearby regions essentially driving the diffusion of water into these regions. For time periods above 70 hours, there does appear to be a lower concentration of water in the "light" grains of the cork compared to the "dark" grains. While this observation is suggestive that there is a variation in the diffusion coefficient between autumn and spring growth grains in the cork, it is difficult to draw a definitive conclusion since the boundary conditions (ie. the water concentration) surrounding the regions of interest are dynamic and not controlled during the experiment.

5 Conclusion

THz time-domain imaging is shown to be a viable non-destructive evaluation tool to measure the local and average diffusion of water in natural cork. In comparison, conventional methods of measuring liquid diffusion in natural cork typically average over the local variations in cork structure. From time-dependant THz images of water concentration, it is clear that lenticels, cracks and voids in the cork strongly influence the local as well as average diffusion properties. Localized measurements of water diffusion are in good agreement with previous observations: (a) channels near the surface quickly absorb water (b) diffusion in the radial growth direction is faster than the non-radial directions.

Beyond the diffusion measurements described in this paper, THz imaging as a non-contact/non-destructive method could enable real-time measurements of liquid diffusion in a variety of configurations. For example, is could be used to measure diffusion of wine into a cork stopper in the neck of a wine bottle. As a technique it could also be used to study the effect of cork structure on the extraction and migration of volatile chemicals, from the cork-wine interface.

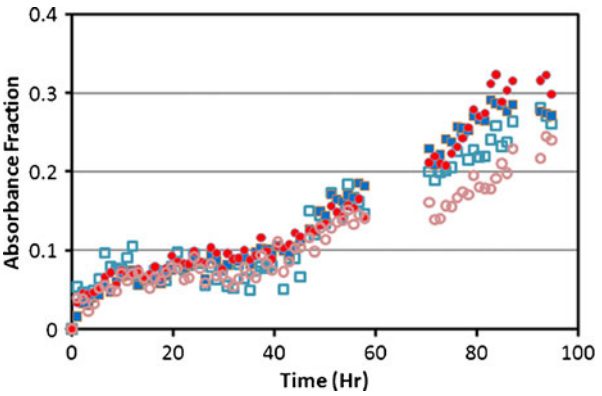

Fig. 14 Absorbance fraction versus time for Region 5 (*open square*), 6 (*solid square*), 7 (*solid circle*) and 8 (*open circle*).

Acknowledgements The authors gratefully acknowledge helpful discussions with M. Cabral and P. Lopes.

References

1. C. Jansen, S. Wietzke, O. Peters, M. Scheller, N. Vieweg, M. Salhi, N. Krumbholz, C. Jordens, T. Hochrein, M. Koch, Appl. Optics 49, E48–E57 (2010)
2. L. Ho, Y. Cuppok, S. Muschert, K. C. Gordon, M. Pepper, Y. Shen, F. Siepmann, J. Siepmann, P. F. Taday, T. Rades, Intern. J. Pharmaceutics, 382, 151–159 (2009).
3. J. F. Federici, B. Schulkin, F. Huang, D. Gary, R. Barat, F. Oliveira, D. Zimdars, Semicond. Sci. Technol., 20, S266–80 (2005).
4. J. F. Federici, D. Gary, R. Barat, Z.-H. Michalopoulou, in *Counter-Terrorism Detection Techniques of Explosives* ed. by Jehuda Yinon. (Elsevier, New York, 2007), p. 323
5. H. S. Chua, P. C. Upadhya, A. D. Haigh, J. Obradovic, A. A. P. Gibson, E. H. Linfield, in Conference Digest of the 2004 Joint 29th International Conference on Infrared and Millimeter Waves and 12th International Conference on Terahertz Electronics (IEEE, New York, 2004), p. 399–400
6. H. S. Chua, J. Obradovic, A. D. Haigh, P. C. Upadhya, O. Hirsch, D. Crawley, A. A. P. Gibson, l. F. Gladden, E. H. Linfield, 2005 IEEE MTT-S International Microwave Symposium. (IEEE, New York, 2005), p. 4.
7. S. Hadjiloucas, L. S. Karatzas, J. W. Bowen, IEEE Trans. Microwave Theory and Techniques, 47, pp. 142–149 (1999)
8. S. Hadjiloucas, R. K. H. Galvao, J. W. Bowen, Opt. Soc. Am. A, 19, pp. 2495–2509 (2002)
9. C. Jordens, M. Scheller, B. Breitenstein, D. Selmar, M. Koch, J. Biological Physics, 35, pp. 255–264 (2009)
10. M. Reid, R. Fedosejevs, Appl. Optics, 45, pp. 2766–2772 (2006).
11. J. Balakrishnan, B. M. Fischer, D. Abbott, Appl. Opt., 48, pp. 2262–2266 (2009)
12. C.Jordens, S. Wietzke, M. Scheller, M. Koch, Polymer Testing, 29, pp. 209–215 (2010).
13. Y. L. Hor, J. F. Federici, R. L. Wample, Appl. Opt., 47, pp. 72–78 (2008)
14. H. Pereira, *Cork: Biology, Production and Uses.* (Elsevier, New York, 2007).
15. M. E. Rosa, M. A. Fortes, Wood and Fiber Science, 25, pp. 339–348 (1993)
16. J. R. Gonzalez-Adrados, F. Gonzalez-Hernandex, J. L. Garcia De Ceca, M. J. Caceres-Esteban, M. C. Carcia-Vallejo, J. Int. Sci. Vigne Vin, 42, pp. 161–166 (2008)
17. J. Obradovic, J. H. P. Collins, O. Hirsch, M. D. Mantle, M. L. Johns, L. F. Gladden, Polymer, 48, pp. 3494–3503 (2007)
18. J. N. Marat-Mendes, E. R. Neagu, Ferroelectrics, 294, pp. 123–131 (2003)
19. A. M. Gil, M. H. Lopes, C. Pascoal Neto, P. T. Callaghan, J. Materials Sci., 35, pp. 1891–1900 (2000).
20. M. Scheller, S. Wietzhe, C. Jansen, M. Koch, J. Phys. D: Appl. Phys., 42, pp. 065415–10 (2009)
21. J. C. Maxwell-Garnett, Phil. Trans. R. Soc. Lond. Ser. A, 206, pp. 385–420 (1904).
22. C. Ronne, L. Thrane, P.-O. Astrand, A. Wallqvist, K. V. Mikkelsen, S. R. Keiding, J. Chem. Phys, 107, pp. 5319–31 (1997).
23. J. Crank, *The Mathematics of Diffusion* (Clarendon, Oxford, 2001)